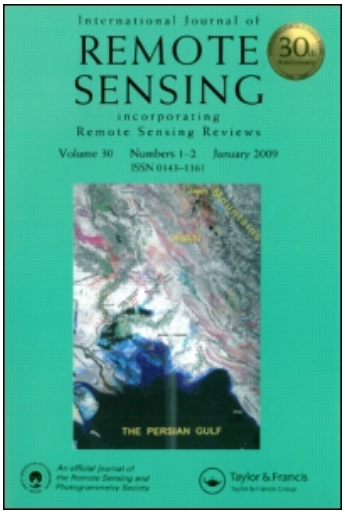

International Journal of Remote Sensing
Publication details, including instructions for authors and subscription information:
http://www.informaworld.com/smpp/title~content=t713722504

Surface latent heat flux and rainfall associated with rapidly intensifying tropical cyclones over the western North Pacific

Si Gao[a]; Long S. CHIU[a]
[a] Institute of Space and Earth Information Science, Chinese University of Hong Kong, Shatin, NT, Hong Kong SAR, PRC

Online publication date: 28 September 2010

To cite this Article Gao, Si and CHIU, Long S.(2010) 'Surface latent heat flux and rainfall associated with rapidly intensifying tropical cyclones over the western North Pacific', International Journal of Remote Sensing, 31: 17, 4699 — 4710
To link to this Article: DOI: 10.1080/01431161.2010.485149
URL: http://dx.doi.org/10.1080/01431161.2010.485149

International Journal of Remote Sensing
Vol. 31, Nos. 17–18, September 2010, 4699–4710

Taylor & Francis
Taylor & Francis Group

Surface latent heat flux and rainfall associated with rapidly intensifying tropical cyclones over the western North Pacific

SI GAO and LONG S. CHIU*
Institute of Space and Earth Information Science, Chinese University of Hong Kong, Shatin, NT, Hong Kong SAR, PRC

This study examines the surface latent heat flux (SLHF) and rainfall associated with rapidly intensifying western North Pacific tropical cyclones (TCs). The mean initial ($t = 0$ h) SLHF conditions of samples that undergo rapid intensification (RI) are compared with those of the non-RI samples for four categories classified by moving direction over a 24-h period. The results show that RI samples are usually associated with an area of relatively high SLHF on the right-hand side of TC track and with relatively high rainfall within inner-core regions. Student *t*-tests show statistically significant differences between SLHF of RI and non-RI samples ahead of the TC track, suggesting that SLHF plays an important role in TC rapid intensification. SLHF and inner-core rainfall have the potential to be new predictors for TC intensity forecasting.

1. Introduction

While significant progress has been made in the prediction of tropical cyclone (TC) track, the prediction of intensity remains a difficult task (DeMaria and Gross 2002). Five-day intensity forecasts have been produced by the Joint Typhoon Warning Center (JTWC) for the western North Pacific since 2003; however, the skill of intensity forecasts still lags that of track forecasts (Knaff *et al.* 2005). Blackerby (2005) examined the accuracy of six statistical and dynamical models of TC intensity guidance techniques for western North Pacific and found that none of the guidance techniques predicted rapid intensification (RI) well; all of the techniques tended to under-forecast maximum intensity.

In general, the inability to forecast RI is consistent with our limited understanding of TC intensity change. In the past, the impact of the ocean (e.g. sea surface temperature (SST), ocean heat content), inner-core processes (e.g. eyewall, inner-core asymmetry, sea spray), and environmental interactions (e.g. vertical wind shear, flow pattern, TC–trough interaction) on TC intensity change have been examined (Kaplan and DeMaria 2003, Yu and Kwon 2005, Ventham and Wang 2007, Yang *et al.* 2007, Mainelli *et al.* 2008). Few studies focused on the surface latent heat flux (SLHF). Conditional instability of the second kind (CISK; Charney and Eliassen 1964) and wind-induced surface heat exchange (WISHE; Emanuel 1986) have been considered as two major mechanisms for cyclone intensification. Rainfall as a proxy of condensational heating is a good indicator of typhoon strength. Rodgers *et al.* (1994) and Chang *et al.* (1995) showed examples that the strength of northwest Pacific typhoon intensity is significantly correlated with rainfall intensity within the inner cores (radius of 110 km from storm centre) of the typhoon. However, few studies have

*Corresponding author. Email: longchiu@cuhk.edu.hk

International Journal of Remote Sensing
ISSN 0143-1161 print/ISSN 1366-5901 online
http://www.tandf.co.uk/journals
DOI: 10.1080/01431161.2010.485149

used rainfall associated with TCs to forecast TC intensification. Surface moisture convergence from the surrounding atmosphere and the underlying sea surface must provide the moisture for condensational heating. Gautam *et al.* (2005) found that the intensification of Hurricane Isabel that occurred in 2003 was associated with strong SLHF along its track. The goal of this study is to quantify the role of SLHF and rainfall in cyclone intensification. We will concentrate on samples when cyclones underwent RI. A composite analysis will be performed for the RI and non-RI samples and the significance of the difference tested using a Student *t*-test.

The dataset and methodology used in this study is described in §2. Section 3 provides the climatology of western North Pacific TC 24-h intensity changes. Composites of the rainfall and SLHF are presented in §4 and §5, respectively. Finally, conclusions and discussions are offered in §6.

2. Data and methodology

2.1 *Data description*

The database used in this study consists of all TCs in western North Pacific basin (including the South China Sea (SCS)) from 1998 to 2006 collected from Japan Meteorological Agency (JMA) Regional Specialized Meteorological Center Tokyo (RSMC Tokyo) best track data. The data consist of 6-h estimates of position, minimum central pressure (MCP), and 10-min maximum sustained wind speed (MWS) for all named western North Pacific and SCS TCs from 1951 to the present.

The rainfall dataset from 1998 to 2006 is the Tropical Rainfall Measuring Mission (TRMM) Multi-satellite Precipitation Analysis (TMPA) (Huffman *et al.* 2007). TMPA provides a calibration-based sequential scheme for combining precipitation estimates from multiple satellites, as well as gauge analyses where feasible, at fine scales ($0.25^\circ \times 0.25^\circ$ and 3-hourly). The data sources from satellites include TRMM Microwave Imager (TMI), Special Sensor Microwave Imager (SSM/I), Advanced Microwave Scanning Radiometer Earth Observing System (EOS) (AMSR-E), Advanced Microwave Sounding Unit-B (AMSU-B), and infrared data of geosynchronous earth orbit satellites. TMPA is available both after and in real time, based on calibration by the TRMM Combined Instrument and TRMM Microwave Imager precipitation products, respectively. Only the after-real-time product incorporates gauge data at the present. The dataset covers the latitude band 50 °N–S for the period from 1998 to the delayed present.

We examined a number of semi-operational SLHF products for this study. Satellite-based products, such as the NASA/Goddard Space Flight Center Satellite-based Surface Turbulent Flux (GSSTF) dataset (Chou *et al.* 1997), the Japanese Ocean Flux utilizing Remote Sensing Observations (J-OFURO) (Kubota *et al.* 2002) and the Hamburg Ocean–Atmospheric Parameter Set (HOAPS) (Grassl *et al.* 2000) are deemed inadequate due to either coarse resolution, missing data around the TC centre or insufficient temporal coverage. The third release of the Objectively Analysed Air–sea Fluxes (OAFlux) (Yu *et al.* 2008) daily SLHF data for the same period were utilized. Both JMA and OAFlux datasets are gridded on a 1.0° latitude–longitude resolution for the global ocean basins that are free from ice. The SLHF, Q_{LH}, is based on the state-of-the-art Coupled Ocean–Atmosphere Response Experiment (COARE) bulk flux algorithm 3.0 (COARE 3.0) (Fairall *et al.* 2003), namely

$$Q_{\mathrm{LH}} = \rho L_{\mathrm{e}} c_{\mathrm{e}} U(q_{\mathrm{s}} - q_{\mathrm{a}}) = \rho L_{\mathrm{e}} c_{\mathrm{e}} U \Delta q \quad (1)$$

where ρ is the density of air, L_{e} is the latent heat of evaporation, c_{e} is the turbulent exchange coefficients for latent heat flux, U is the wind speed relative to the sea surface at the height of 10 m, $\Delta q = q_{\mathrm{s}} - q_{\mathrm{a}}$ where q_{s} and q_{a} denote the surface and near-surface (i.e. 2 m) atmospheric specific humidity, respectively. q_{s} is computed from the saturation humidity, q_{sat}, for pure water at SST T_{s},

$$q_s = 0.98 q_{\mathrm{sat}}(T_{\mathrm{s}}) \quad (2)$$

where a multiplier factor of 0.98 is used to take into account the reduction in vapour pressure caused by a typical salinity of 34 psu. It is worth pointing out that the extrapolated values of c_{e} in COARE 3.0 from 19 to 36 m s^{-1} are in good agreement with the results form Coupled Boundary Layer Air–Sea Transfer Experiment (CBLAST) (Black *et al.* 2007) and Humidity Exchange over the Sea Experiment (HEXOS) (DeCosmo *et al.* 1996; modified as per Fairall *et al.* (2003)). This suggests that c_{e} is constant with wind speed up to hurricane-force winds of 33 m s^{-1}.

The OAFlux SLHF product is different from other flux products in that it is not constructed from one single data source, but rather it is determined by objectively blending the data sources from satellite and numerical weather prediction (NWP) model outputs while using *in situ* observations to assign the weights. Input data sources for the synthesis included satellite retrievals from SSM/I, the Quick Scatterometer (QuikSCAT), Advanced Very High Resolution Radiometer (AVHRR), TMI, AMSR-E, and surface meteorological data from the European Centre for Medium-Range Weather Forecasts (ECMWF) operational forecast analysis, the 40-year ECMWF Re-Analysis (ERA-40), and the National Centers for Environmental Prediction (NCEP) reanalysis. Consistent with the NWP model outputs, the synthesis produced U at 10 m, q_{a} at 2 m, and T_{s} at the sea surface. A height adjustment was applied to those input datasets that do not have the specified reference heights.

Although this is an analysed product, the initial SLHF fields are specified by the input parameters, hence prediction is possible using this product.

2.2 *Methodology*

Variables were evaluated at the beginning ($t = 0$ h) of each 24-h period provided that the system remained both over water and tropical (e.g. extra-tropical samples were excluded and landfall effect was left out of account) during a 24-h period. The 24-h intensity change in MCP (ΔP_{24}) were determined for each 24-h time period by subtracting MCP at $t + 24$ h from MCP at the initial ($t = 0$ h) time.

There were 209 named TCs (91 tropical storms (17.2 m s^{-1} $\leq$ MWS $\leq$ 32.6 m s^{-1}) and 118 typhoons (MWS $\geq$ 32.7 m s^{-1})). It should be noted that the TCs are defined based on the maximum intensity during the life of the TCs, hence no tropical depressions (MWS $\leq$ 17.1 m s^{-1}) are recorded in the dataset. These TCs contributed a total of 5077 samples (e.g. 24-h period differences) that were subsequently employed in the statistical analyses discussed in §3 and §4.

To determine if SLHF conditions associated with the RI samples were significantly different from those non-RI samples, a composite analysis on initial ($t = 0$ h) rainfall and SLHF characteristics in a 20° × 20° square region centred at TC position for RI samples and non-RI samples was utilized. Student t-tests (Bulmer 1979) were used to perform significance tests for the difference between RI and non-RI samples.

3. Intensity change distribution

Figure 1 shows the frequency distribution of ΔP_{24} as a function of the initial ($t = 0$ h) intensity of all 5077 samples. Slow intensification (–9 mb $\leq \Delta P_{24} \leq 0$) was the most frequently observed 24-h intensity change for tropical depressions. The figure indicates that a higher fraction of the tropical storm sample than of the typhoon or tropical depression sample exhibited ΔP_{24} fall exceeding 10 mb. This finding may be attributed to several factors, as Kaplan and DeMaria (2003) proposed. First, tropical storms are further from their maximum potential intensity than typhoons and, consequently, have the potential to intensify faster. Second, tropical storms may intensify more rapidly than tropical depressions because they are better organized. Conversely, figure 1 indicates that typhoons are likely to decay at a faster rate than either tropical storms or tropical depressions, because of their high intensities.

The cumulative frequency distribution of ΔP_{24} for each intensity category (not shown) indicates that TC decay ($\Delta P_{24} > 0$) occurs for ~70% of all typhoon samples: however, it only occurs in 17% of the tropical depression samples, 43% of the tropical storm samples, and 44% of all TC samples.

To separate RI and non-RI samples, RI is defined as the 90th percentile of ΔP_{24} for all of the TC samples used in this study. Correspondingly, samples with ΔP_{24} fall ≥ 20 mb are RI samples and the others are non-RI samples. It is interesting to note that the Holliday and Thompson's (1979) definition for RI of a 24-h pressure fall of ≥ 42 mb is equivalent to the 98.8th percentile of all of the 24-h pressure changes of the TCs in the current study sample.

The percentage of systems that underwent RI at least once during their lifetime is also analysed. Our result shows that 86% of all typhoons and 95% of all super-typhoons (MWS ≥ 51 m s^{-1}) underwent RI at least once during their lifetime. Overall, 51% of all named western North Pacific TCs underwent RI during their life time.

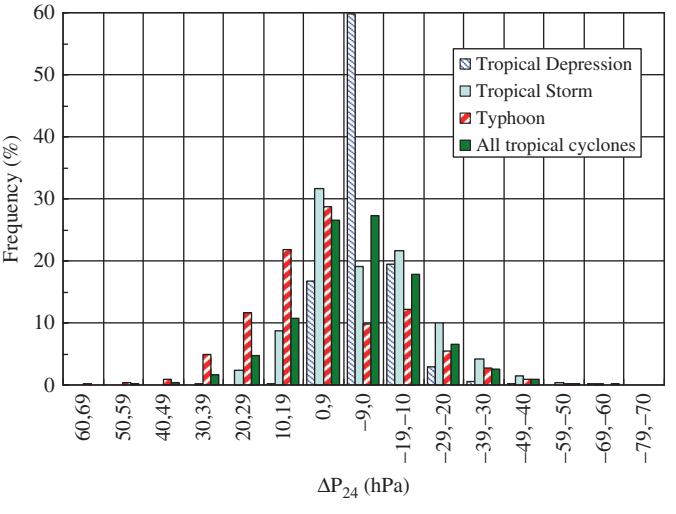

Figure 1. The frequency distributions of 24-h intensity change (ΔP_{24}) stratified by TC intensity at time $t = 0$ h. The distributions are provided for tropical depressions, tropical storms, typhoons, and all TCs.

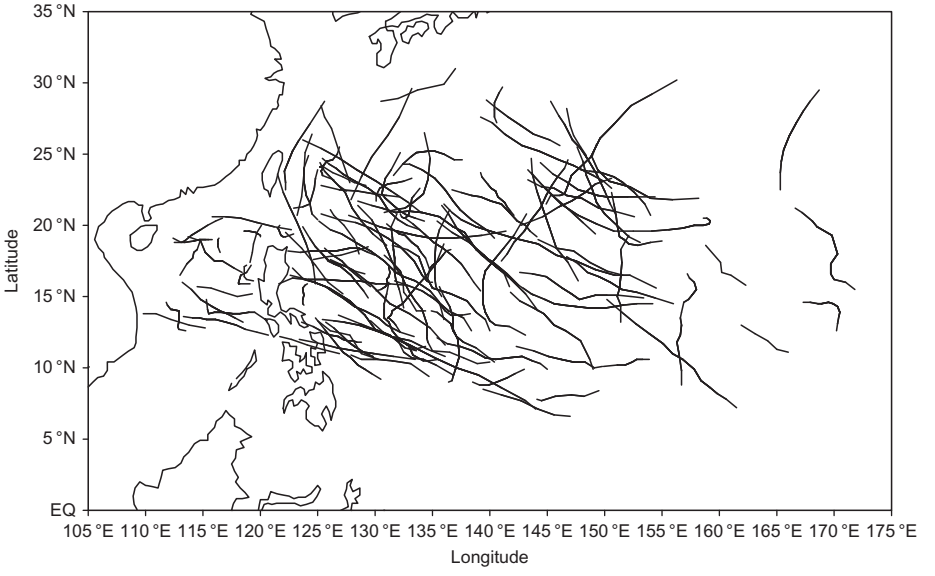

Figure 2. The 24-h tracks of the 1998–2006 RI samples.

Figure 2 shows the 24-h tracks of the RI samples. Because RI may occur continuously over a 24-h time periods, some of the tracks overlap. The figure shows that RI generally occurred in regions between 10° N and 25° N. There was no RI case occurring in coastal ocean area with exceptions for those in the vicinity of Taiwan and the Philippines. The lowest latitude for RI is 7° N. Both Taiwan and the Philippines are surrounded by open sea which is favourable for RI. At latitudes too close to the equator (5° N to 5° S), the small Coriolis parameter does not provide enough Coriolis force favourable for RI.

Figure 3 shows the seasonal distribution of the RI samples. The vast majority of the RI samples (73%) occurred from July to October, and RI occurred most frequently in September. This is a slight delay for the RI compared to that in the Atlantic (Kaplan and DeMaria 2003), which shows the vast majority of the RI samples occur in August and September.

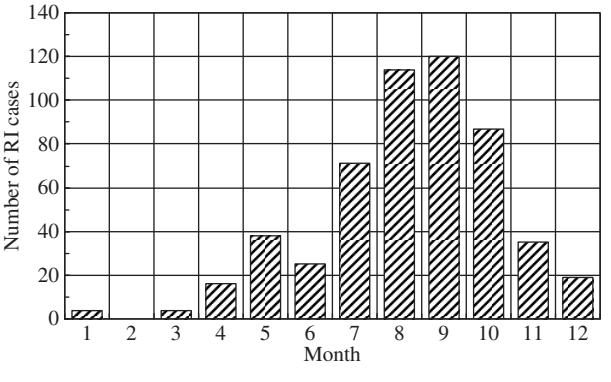

Figure 3. The seasonal distribution of RI samples (1998–2006).

4. Rainfall pattern

In this section, the rainfall distributions at the start of each of the RI samples are compared to the non-RI samples. Each sample corresponds to a 24-h displacement. Figure 4 shows the composite of rainfall for RI samples, non-RI samples, and their difference. The areas with statistically significant difference at 95% confidence level determined by a *t*-test are shaded.

It is seen clearly from figure 4 that composite rainfall of RI samples is higher than that of non-RI samples in the areas near TC centre, with a maximum of ~6.5 mm h^{-1} within inner-core regions compared to ~4.0 mm h^{-1} for non-RI samples.

5. SLHF

In this section, the SLHF conditions present at the start of each of the RI samples are compared with the non-RI samples. Figure 5 shows the composite of SLHF for RI samples, non-RI samples, and their difference for all the samples. The areas with statistically significant difference at 95% confidence level determined by a *t*-test are shaded. The SLHF associated with RI samples tend to be higher than the non-RI samples, with a maximum of ~190 W m^{-2} to the north of the TC centre compared with ~150 W m^{-2} to the north of the TC centre for the non-RI samples. There is significant difference between RI and non-RI samples to the north of TC centre.

The pattern of high SLHF to the north of the TC centre for RI samples suggests there is directionality of SLHF for RI. Hence all samples are divided into four categories according to the TC moving direction over each 24-h time period (see figure 6). Table 1 summarizes the number of RI and non-RI 24-h displacement samples for each direction. Overall there is a roughly 1 in 9 (10.9%) chance for RI. The chance for RI is the highest for northwestward moving samples (13.3%) and the least for northeastward moving samples (6.1%), with comparable chance for westward and northward moving samples (12.2% and 9.1%, respectively).

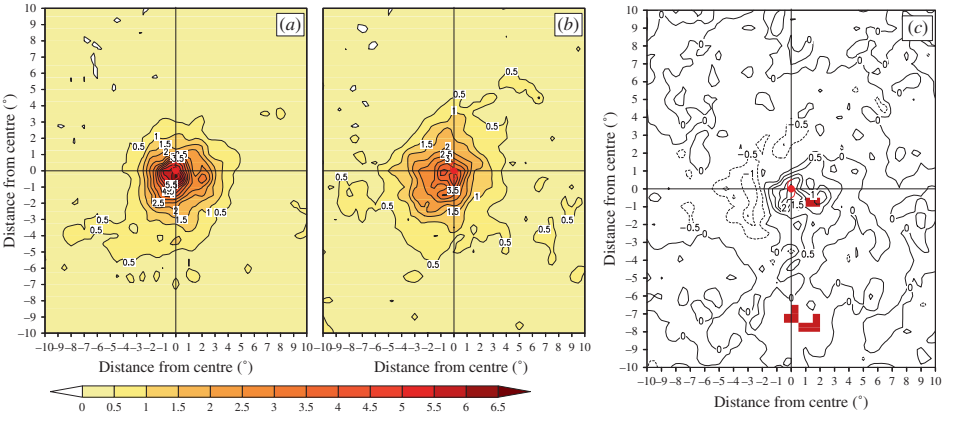

Figure 4. The composite initial rainfall distribution of: (*a*) RI samples; (*b*) non-RI samples; (*c*) difference between RI and non-RI samples (RI samples – non-RI samples) for all the samples. Areas with statistically significant difference at the 95% confidence level are shaded. The origin denotes the TC centre at $t = 0$ h. The x and y ordinates represent east and north, respectively (unit: mm h^{-1}).

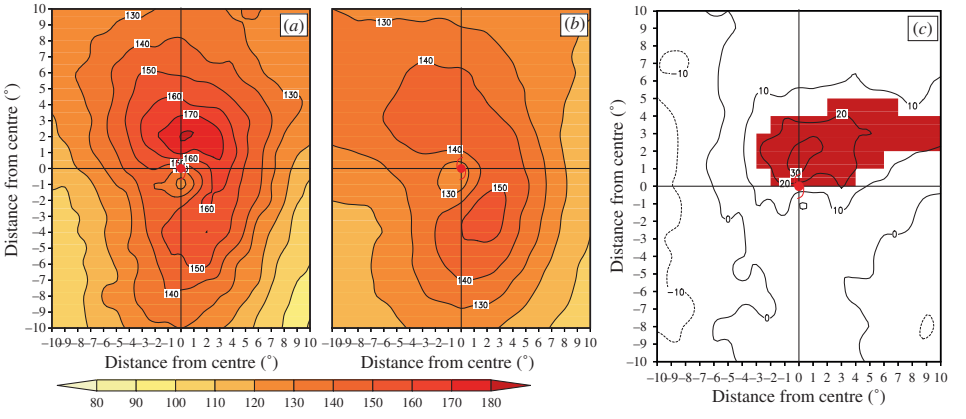

Figure 5. Same as figure 4 except for SLHF (unit: W m^{-2}).

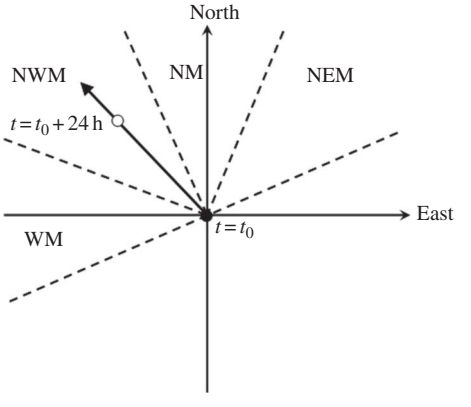

Figure 6. Four categories based on moving direction: westward moving category (WM), northwestward moving category (NWM), northward moving category (NM), northeastward moving category (NEM). The filled circle and the open circle denote TC positions at $t = t_0$ and at $t = t_0 + 24$ h, respectively. Each of the four angles is 45°.

Table 1. The sample sizes of four categories stratified by moving direction. The number of RI and non-RI samples and the percentage of RI samples for each category are also presented.

	Total sample number (%)	RI	Non-RI	Per cent RI
Westward moving	1263 (26.9)	154	1109	12.2
Northwestward moving	1706 (32.3)	227	1479	13.3
Northward moving	786 (16.7)	72	714	9.1
Northeastward moving	945 (20.1)	58	887	6.1
All	4700 (100.0)	511	4189	10.9

Composite analyses on SLHF were performed for the overall samples first and then for each moving directions separately. Figure 7 shows the composite of SLHF for RI samples, non-RI samples, and their difference for westward moving category. The

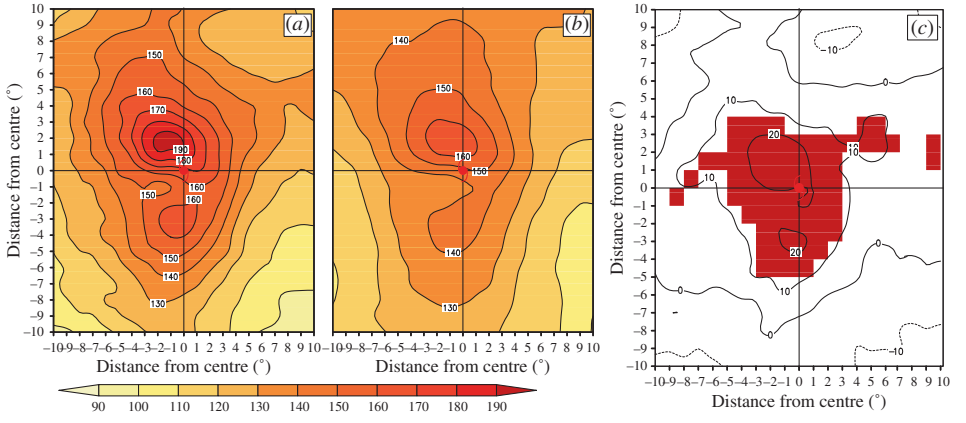

Figure 7. Same as figure 5 except for westward moving category.

areas with statistically significant difference at 95% confidence level determined by a *t*-test are shaded. The SLHF associated with RI samples tend to be higher than the non-RI samples, with a maximum to the north–northwest of the TC centre of ~190 W m^{-2} compared with ~160 W m^{-2} for the non-RI samples. The maximum SLHF is roughly located to the right of the moving direction for both RI and non-RI samples. A significant difference between RI and non-RI samples exists for an area around the TC centres (figure 5(*c*)).

For northwestward moving category the maxima of ~180 W m^{-2} for RI samples (figure 8(*a*)) and ~170 W m^{-2} for non-RI samples (figure 8(*b*)) shift to the north of the TC centre, and the maximum is also located roughly on the right-hand side of the moving direction. The significant difference between RI and non-RI samples exists over an area to the northwest of the TC centres (figure 8(*c*)).

Figure 9 is similar to figure 7, except it is for the northward moving category. The maxima of ~180 W m^{-2} for RI samples (figure 9(*a*)) and ~170 W m^{-2} for non-RI samples (figure 9(*b*)) shift to the east of the TC centre, and the maximum is also

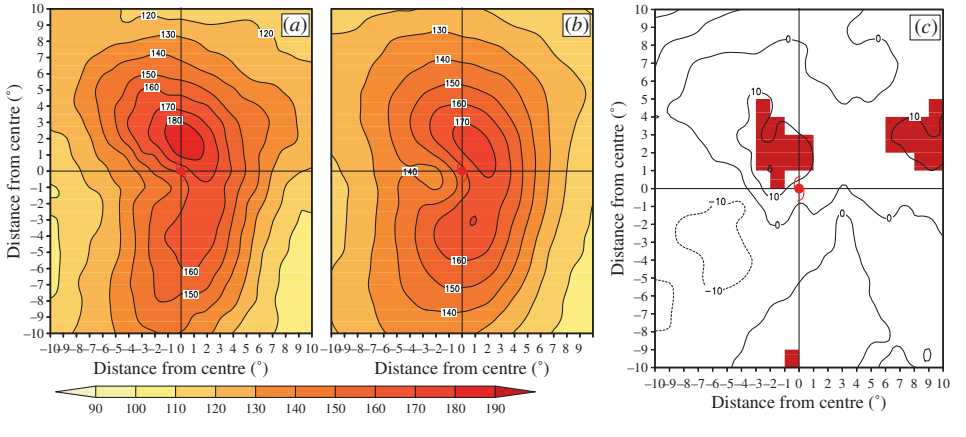

Figure 8. Same as figure 5 except for northwestward moving category.

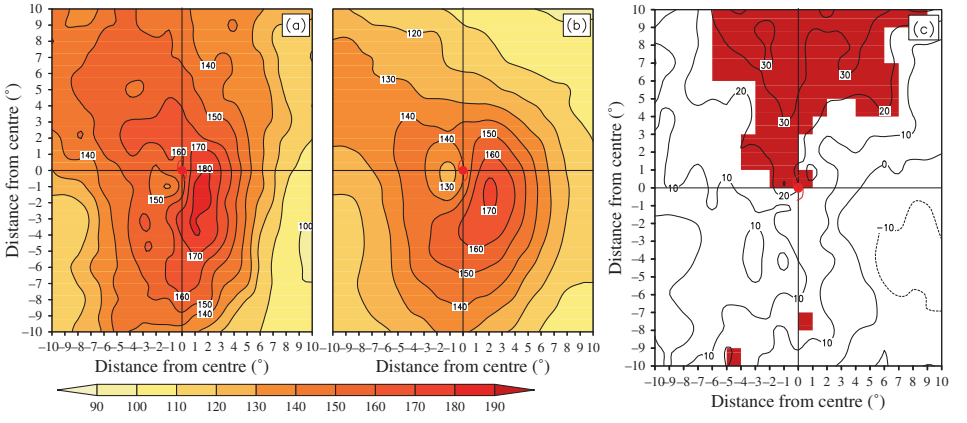

Figure 9. Same as figure 5 except for northward moving category.

located roughly on the right-hand side of moving direction. The significant difference between RI and non-RI samples exists over an area to the north of the TC centres (figure 9(*c*)).

For the northeastward moving category there exists maxima of ~170 W m^{-2} for RI samples (figure 10(*a*)) and ~150 W m^{-2} for non-RI samples (figure 10(*b*)), both on the right-hand side of moving direction; and there are maxima to the northwest of the TC centres for both RI and non-RI samples, where the difference of SLHF between RI and non-RI samples is not significant. The significant difference does exist over an area to the northeast of the TC centres (figure 10(*c*)).

The maxima of SLHF located on the right-hand side of TC track for all the four categories are mainly due to the cyclonic circulation of TC that results in the largest resultant wind speed on the right-hand side, because they move in the same direction on the right-hand side of TC. These results demonstrate that TCs that move to higher SLHF areas tend to intensify rapidly, suggesting that SLHF provides the energy and moisture for TC RI.

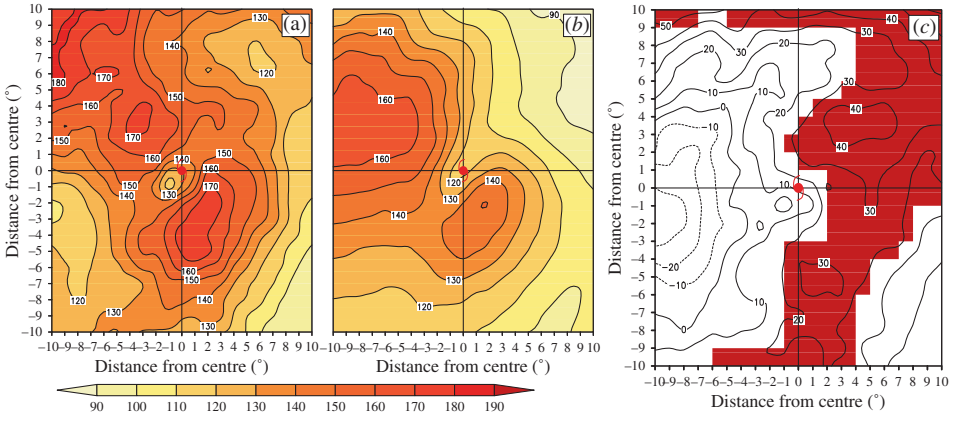

Figure 10. Same as figure 5 except for northeastward moving category.

6. Conclusion and discussion

The primary findings of this study are as follows.

(*a*) In this study, RI was defined as approximately the 90th percentile of all 24-h over-water intensity changes of western North Pacific and South China Sea TCs from 1998 to 2006. This is equal to a minimum central pressure fall of 20 mb over a 24-h period.

(*b*) Of the 209 named TCs that comprise the 1998–2006 samples, 51% of all named TCs, 86% of all typhoons, and 95% of super typhoons undergo RI at least once during their lifetime.

(*c*) The rainfall within inner-core regions of RI samples is higher than that of non-RI samples.

(*d*) The SLHF associated with RI and non-RI samples show general similar patterns for all four categories. There are maxima of SLHF to the right of TC track. The significant difference of SLHF for RI and non-RI samples occurs on TCs' pathway, suggesting that SLHF, which provide moisture and energy from ocean surface for TC development, is an important factor in TC RI.

The inner-core rainfall of storms is a good indicator of the latent heat release, which is a crucial heat source for storm intensification. The case studies on Hurricane Isidore and Lili (2002) (Jiang *et al.* 2008) demonstrated that the inner-core mean rain rate peaks (convective bursts) appear to precede the times of maximum surface winds. This inner-core rain peak and intensity relationship was also revealed in satellite and aircraft observation studies of Typhoon Lynn (1987) (Rao and Macarthur 1994), Typhoon Bobbie (1992) (Rodgers and Pierce 1995), Hurricane Opal (1995) (Rodgers *et al.* 1998), Typhoon Paka (1997) (Rodgers *et al.* 2000), and Hurricane Bonnie (1998) (Heymsfield *et al.* 2001), as well as in observational studies of Hurricane Daisy (1958) (Riehl and Malkus 1961) and Tropical Cyclone Oliver (1993) (Simpson *et al.* 1998).

SLHF is a nonlinear combination of U and the difference of q_s and q_a, where q_s depends on SST. Although SST has been utilized to estimate the maximum potential intensity (MPI), which is already a predictor in statistical typhoon intensity prediction scheme (Knaff *et al.* 2005), our result shows that SLHF and inner-core rainfall have the potential to be new predictors for TC intensity forecasting. Future work will focus on investigating whether SLHF and inner-core rainfall can be employed to improve the intensity forecast, especially for RI estimates. Besides multiple linear regression method, more sophisticated statistical techniques, such as neural networks, will also be employed in future studies.

Acknowledgement

This work is supported by a Direct Grant no. 2020925 from the Chinese University of Hong Kong.

References

Blackerby, J.S., 2005, Accuracy of western North Pacific tropical cyclone intensity guidance. MS thesis, Naval Postgraduate School, USA

Black, P.G., D'Asaro, E.A., Drennan, W.M., French, J.R., Niiler, P.P., Sanford, T.B., Terrill, E.J. and Zhang, J.A., 2007, Air–sea exchange in hurricanes: synthesis of observations from the Coupled Boundary Layer Air–Sea Transfer Experiment. *Bulletin of the American Meteorological Society*, **88**, pp. 357–374.

Bulmer, M.G., 1979, *Principles of Statistics* (New York: Dover Publications).

CHANG, A.T.C., CHIU, L.S., LIU, G.R. and WANG, K.H., 1995, Analysis of 1994 typhoons in the Taiwan region using satellite data. In *COSPAR Colloquia Series Volume 8, Space Remote Sensing of Subtropical Oceans*, SRSSO, Taipei, Taiwan (Amsterdam: Elsevier Science), pp. 89–96.

CHARNEY, J.G. and ELIASSEN, A., 1964, On the growth of the hurricane depression. *Journal of the Atmospheric Sciences*, **21**, pp. 68–75.

CHOU, S.H., SHIE, C.L., ATLAS, R.M. and ARDIZZONE, J., 1997, Air–sea fluxes retrieved from special sensor microwave imager data. *Journal of Geophysical Research*, **102**, pp. 12706–12726.

DE COSMO, J., KATSAROS, K.B., SMITH, S.D., ANDERSON, R.J., OOST, W.A., BUMKE, K. and CHADWICK, H., 1996, Air-sea exchange of water vapour and sensible heat: The Humidity Exchange of the Sea (HEXOS) results. *Journal of Geophysical Research*, **101**, pp. 12001–12016.

DEMARIA, M. and GROSS, J.M., 2003, Evolution of prediction models. In *Hurricane!: Coping with Disaster*, R. Simpson (Ed.), pp. 103–126 (Washington, DC: American Geophysical Union).

EMANUEL, K.A., 1986, An air–sea interaction theory for tropical cyclones. Part I: Steady-state maintenance. *Journal of the Atmospheric Sciences*, **43**, pp. 585–605.

FAIRALL, C.W., BRADLEY, E.F., HARE, J.E., GRACHEV, A.A. and EDSON J.B., 2003, Bulk parameterization on air–sea fluxes: updates and verification for the COARE algorithm. *Journal of Climate*, **16**, pp. 571–591.

GAUTAM, R., CERVONE, G., SINGH, R.P. and KAFATOS, M., 2005, Characteristics of meteorological parameters associated with Hurricane Isabel. *Geophysical Research Letters*, **32**, L04801, doi:10.1029/2004GL021559.

GRASSL, H., JOST, V., KUMAR, R., SCHULZ, J., BAUER, P. and SCHLUESSEL, P., 2000, The Hamburg Ocean Atmosphere Parameters and fluxes from Satellite data (HOAPS): a climatological atlas of satellite derived air sea interaction parameters over the Oceans. Report No. 312, ISSN 0937-1060, Max Planck Institute for Meteorology, Hamburg, Germany.

HEYMSFIELD, G.M., HALVERSON, J.B., SIMPSON, J., TIAN, L. and BUI, T.P., 2001, ER-2 Doppler radar investigations of the eyewall of Hurricane Bonnie during the Convection and Moisture Experiment-3. *Journal of Applied Meteorology*, **40**, pp. 1310–1330.

HUFFMAN, G.J., ADLER, R.F., BOLVIN, D.T., GU, G., NELKIN, E.J., BOWMAN, K.P., HONG, Y., STOCKER, E.F. and WOLFF, D.B., 2007, The TRMM Multisatellite Precipitation Analysis (TMPA): quasi-global, multiyear, combined-sensor precipitation estimates at fine scales. *Journal of Hydrometeorology*, **8**, pp. 38–55.

HOLLIDAY, C.R. and THOMPSON, A.H., 1979, Climatological characteristics of rapidly intensifying typhoons. *Monthly Weather Review*, **107**, pp. 1022–1034.

JIANG, H., HALVERSON, J.B. and SIMPSON, J., 2008, On the differences in storm rainfall from hurricanes Isidore and Lili. Part I: satellite observations and rain potential. *Weather Forecasting*, **23**, pp. 29–43.

KAPLAN, J. and DEMARIA, M, 2003, Large-scale characteristics of rapidly intensifying tropical cyclones in the North Atlantic basin. *Weather Forecasting*, **18**, pp. 1093–1108.

KNAFF, J.A., SAMPSON, C.R. and DEMARIA, M., 2005, An operational statistical typhoon intensity prediction scheme for the Western North Pacific. *Weather Forecasting*, **20**, pp. 688–699.

KUBOTA, M., IWASAKA, N., KIZU, S. and KNODA, M., 2002, Japanese Ocean Flux Data Sets with Use of Remote Sensing Observations (J-OFURO). *Journal of Oceanography*, **58**, pp. 213–225.

MAINELLI, M., DEMARIA, M., SHAY, L.K. and GONI, G., 2008, Application of oceanic heat content estimation to operational forecasting of recent Atlantic category 5 hurricanes. *Weather Forecasting*, **23**, pp. 3–16.

RAO, G.V. and MACARTHUR, P.D., 1994, The SSM/I estimated rainfall amounts of tropical cyclones and their potential in predicting the cyclone intensity changes. *Monthly Weather Review*, **122**, pp. 1568–1574.

RIEHL, H. and MALKUS, J., 1961, Some aspects of Hurricane Daisy, 1958. *Tellus*, **13**, pp. 181–213.

RODGERS, E.B., CHANG, S.W. and PIERCE, H.F., 1994, A satellite observational and numerical study of the precipitation characteristics in western north Atlantic tropical cyclones. *Journal of Applied Meteorology*, **33**, pp. 573–593.

RODGERS, E.B. and PIERCE, H.F., 1995, Environmental influence on Typhoon Bobbie's precipitation distribution. *Journal of Applied Meteorology*, **34**, pp. 2515–2532.

RODGERS, E.B., OLSON, W.S., KARYAMPUDI, V.M. and PIERCE, H.F., 1998, Satellite-derived latent heating distribution and environmental influences in Hurricane Opal (1995). *Monthly Weather Review*, **126**, pp. 1229–1247.

RODGERS, E.B., OLSON, W.S., HALVERSON, J., SIMPSON, J. and PIERCE, H.F., 2000, Environmental forcing of Supertyphoon Paka's (1997) latent heat structure. *Journal of Applied Meteorology*, **39**, pp. 1983–2006.

SIMPSON, J., HALVERSON, J.B., FERRIER, B.S., PATERSEN, W.A., SIMPSON, R.H., BLAKESLEE, R. and DURDEN, S.L., 1998, On the role of 'hot towers' in tropical cyclone formation. *Meteorology and Atmospheric Physics*, **67**, pp. 15–35.

VENTHAM, J.D. and WANG, B., 2007, Large scale flow patterns and their influence on the intensification rates of western North Pacific tropical storms. *Monthly Weather Review*, **135**, pp. 1110–1127.

YANG, B., WANG, Y. and WANG, B., 2007, The effect of internally generated inner-core asymmetries on tropical cyclone potential intensity. *Journal of the Atmospheric Sciences*, **64**, pp. 1165–1188.

YU, H. and KWON, H.J., 2005, Effect of TC–trough interaction on the intensity change of two typhoons. *Weather Forecasting*, **20**, pp. 199–211.

YU, L., JIN, X. and WELLER, R.A., 2008, Multidecade Global Flux Datasets from the Objectively Analyzed Air–sea Fluxes (OAFlux) Project: latent and sensible heat fluxes, ocean evaporation, and related surface meteorological variables. Woods Hole Oceanographic Institution, OAFlux Project Technical Report. OA-2008-01, 64 pp, Woods Hole, Massachusetts.